

REALIZING A SINGLE-STAGE HYBRID PV SYSTEM USING BATTERY CURRENT-SHARING POWER DECOUPLING METHOD

¹Pujari Harish Kumar,²Marathi Rakesh Kumar, ³Dr.Manda Sreedhar,⁴Lingutla Ramesh Naidu

^{1,2}Assistant Professor, Department Of EEE, Tadipatri Engineering College, Tadipatri,AP

³Professor, Department Of EEE, Tadipatri Engineering College, Tadipatri,AP

⁴Associate Professor, Department Of EEE, Tadipatri Engineering College, Tadipatri,AP

ABSTRACT:

Conventionally, the single-stage grid-connected PV inverter needs a large PV-side electrolytic capacitor to suppress the double-line frequency current ripple to keep the PV operating at maximum power point (MPP). However, the short lifetime electrolytic capacitor will reduce the PV inverter’s reliability dramatically. In order to overcome the above problem, a novel battery current-sharing power decoupling (BCSPD) method for hybrid photovoltaic (PV) power systems is proposed in this paper. The proposed BCSPD circuit is parallel-connected with the string PV module to achieve as a single-stage topology. Thus, a high power conversation efficiency can be obtained. The current-injection method is adapted to solve the current ripple problem. Therefore, the required capacitance in PV side can be greatly reduced, so long-life film capacitors can be used instead of electrolytic capacitors. In addition, the battery storage system with the droop control is also used to realize the power regulation function to meet the requirements of actual applications. A 1200 W prototype was designed and implemented to assess the system performance. Experimental results show that the proposed system can track MPP, regulate the load power condition, and reduce current ripple.

INDEX TERMS: Current-Shared; Maximum power point tracking; Photovoltaic power system.

I. INTRODUCTION

In recent years, the grid-connected photovoltaic (PV) power system has been developed dramatically and gradually forms a considerable part of the main grid because of the environmental concern and continuous depletion of fossil fuel reserves. Conventionally, string of PV modules is serially connected to a high enough voltage and connected to a PV inverter (i.e., a grid-connected PV inverter). The traditional PV inverter is divided into single-stage and twostage [1–5]. The single-stage PV inverter has a high-power conversion efficiency as shown in Figure 1. Unfortunately, the single-stage PV inverter has a double-line-frequency current ripple in the PV side [6,7]. In order to briefly describe the double-line-frequency current ripple phenomenon, assume that the grid voltage (t) and the injected current i_o(t) are given as (1) and (2).

$$v_o(t) = V_m \cos(\omega_0 t) \tag{1}$$

$$i_o(t) = I \cos(\omega_0 t) \tag{2}$$

Where ω_0 is the line frequency, V_m is the line peak voltage, and I is the injected peak current. The instantaneous output power (t) can be shown as (3).

$$p_o(t) = v_o(t) \times i_o(t) = \frac{1}{2} V_m I + \frac{1}{2} V_m I \cos(2\omega_0 t) \tag{3}$$

By ignoring the losses in the inverter, the power generated by the PV panel will be equal to the output power (t). This means that there is a significant and huge double-linefrequency ripple current in the PV panel. Therefore, the operating point cannot be maintained at the maximum power point (MPP) as shown in Figure 2. This results in a significant reduction in PV panel output power.

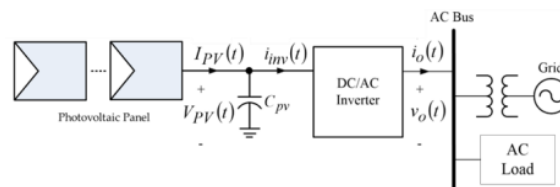


FIGURE 1. The single-state PV inverter

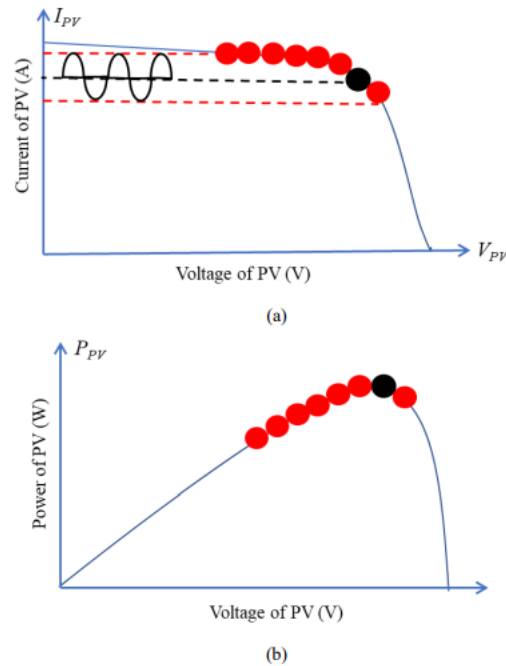


FIGURE 2. The effect of ripple current on (a) VI curve and (b) VP curve

A usual solution to reduce the double-line-frequency current ripple is to use a large electrolytic capacitor (i.e., decoupling capacitor C_{pv} as shown in Figure 1) at the DC link to buffer the ripple power. However, the short lifetime electrolytic capacitor will reduce the PV inverter’s reliability dramatically, and weight and volume are obviously increased. Thus, the two-stage topology, as shown in Figure 3, was used to avoid the current ripple problem at the PV side [8-10]. However, the cost, weight, volume and efficiency of a two-stage topology are worse than that of a single-stage topology. Furthermore, the typical two-stage topology cannot comply with the European standards EN50160, which stipulate that the low frequency voltage pulsation of the DC bus voltage should be kept within the range of 2%.

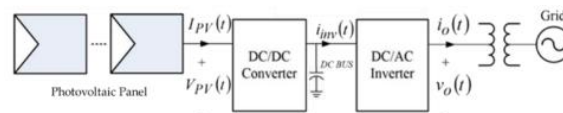


FIGURE 3. The two-stage PV power system

In the other method, active decoupling circuits connected at the PV side or AC side were proposed to sink the ripple current [8,11-15]. This kind of active power decoupling technique utilizes auxiliary power electronic circuits to pump/sink the ripple power into small film capacitors which can be used to replace the large electrolytic capacitor. Although active power decoupling techniques can effectively suppress the ripple current, they increase circuit complexity and cost.

In reality, sunlight is not constant, and the loads and PV power are often mismatched. When much more energy being is produced in the PVs than is being consumed by the loads, the grid will fluctuate [16]. The droop control PV inverter was used to overcome this problem [17,18]. However, generated energy of the PV modules is wasted. Therefore, a hybrid PV power system (i.e., grid-connected PV inverter with battery storage system), shown as Figure 4, was suggested to store the extra power in the battery and then smoothly inject power to the grid to solve this problem [19,20]. Battery storage systems assist in performing one or more important tasks such as (i) smoothing power fluctuation [21,22], (ii) shift peak generation period, and (iii) protection during outages when installed along with large PV generation.

The regulation current i_{cr} is the input current of the proposed BCSPD circuit. According to a typical buck converter theory, the input current is the D times of the inductor current. Thus, the regulation current i_{cr} can be defined as

$$i_{cr} = i_L \cdot D = \frac{V_{PV}D - V_b}{L \cdot f_s} \cdot D \tag{5}$$

From (5), we can know that the regulation current i_{cr} is positive to charge battery When $D > (V_b / V_{PV})$. Oppositely, the regulation current i_{cr} is negative to discharge battery when $D < (V_b / V_{PV})$.

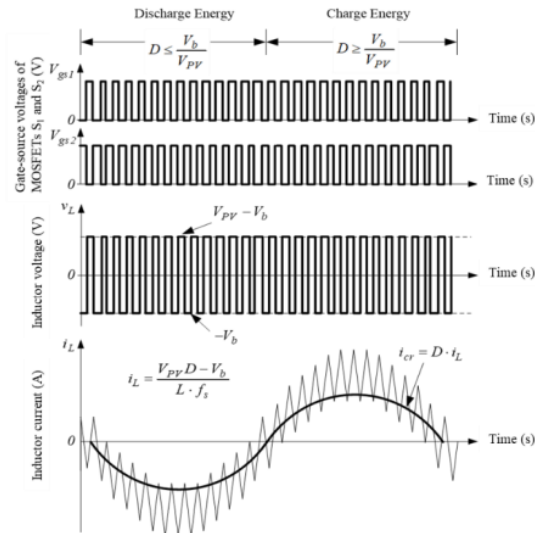


FIGURE 6. The waveforms of the proposed BCSPD circuit

From (2), the proposed BCSPD circuit can be viewed as a controllable current source. The dc/ac inverter with load can be view as a variable current load and shown as

$$i_{inv}(t) = \frac{v_{o,rms} \cdot i_{o,rms} \cdot (1 - \cos 2\omega t)}{V_{PV}} \tag{6}$$

Where,

V_{PV} is the PV module output voltage (V),

$V_{o,rms}$ is the rms values of the AC bus voltage (V),

$I_{o,rms}$ is the rms values of the inverter injecting current (A), and

ω is the grid frequency.

Thus, the simplified model can be plotted as Figure 7. In which, the model of PV module equals a PN junction semiconductor when sunlight can produce a current source PV I .

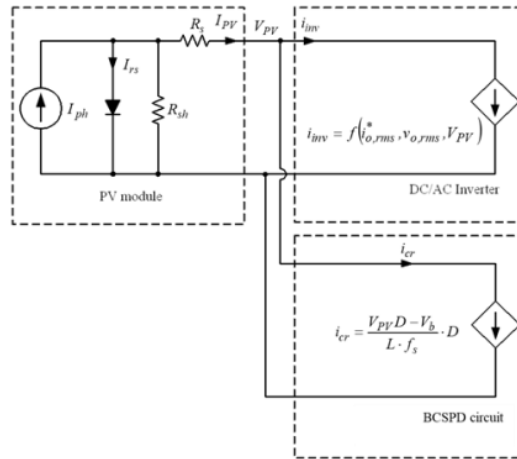


FIGURE 7. The simplified model of the proposed BCSPD circuit for PV power applications

Figure 8 shows the flowchart of the proposed system. First, the root-mean-square (rms) of the grid voltage $v_{o,rms}$ is measured. Then the rms value of the injecting current $i_{o,rms}^*$ can be decided by the droop control method to realize the power regulation.

III. DESIGN CONSIDERATION

There are two kinds of current ripple influence the MPPT. One is the PWM switching current ripple (i.e., high frequency current ripple) from the BCSPD circuit, the other one is the twice utility frequency current ripple (i.e., low frequency current ripple). In order to reduce the high frequency current ripple, the input capacitor C_i is used, and its value can be decided by

$$C_i \geq \frac{I_{cr,max}}{2 \cdot V_{PV} \cdot r \cdot f}$$

where r is the ripple factor.

In order to ensure that the proposed BCSPD circuit can provide the required compensation current of the low frequency current ripple. The small signal analysis is used to check the system control loop stability and frequency response. Figure 11 is the control loop of the proposed system. In which, the $T_p(s)$, $T_c(s)$, and f_k are the transfer functions of the bidirectional converter, the compensation circuit and the feedback gain. The transfer function $T_p(s)$ can be written as

$$T_p(s) = \left. \frac{\tilde{i}_{cr}(s)}{\tilde{v}_{ctr}(s)} \right|_{\tilde{v}_b(s)=0} = \frac{1}{V_r} \times \frac{sL I_b + V_b}{r_s L C_i \left(s^2 + \frac{1}{r_s C_i} s + \frac{D^2}{L C_i} \right)}$$

where

\tilde{v}_b is the small signal of the battery voltage (V),

V_r is the sawtooth waveform with amplitude (V),

I_b is the average battery current (A),

r_s is the internal resistance of the battery (Ω), and

C_i is the input capacitance of the bidirectional DC/DC converter (F).

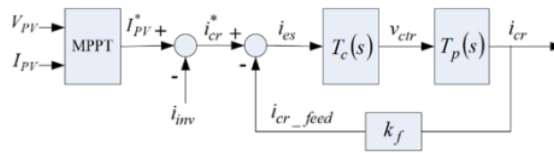


FIGURE 9. The control loop

$$\text{Zero: } f_{Tp_z} = \frac{V_b}{2\pi LI_b} \tag{10}$$

$$\text{Pole: } f_{Tp_p1} = \frac{\left(\frac{1}{r_s C_i} - \sqrt{\left(\frac{1}{r_s C_i} \right)^2 - \frac{4D^2}{LC_i}} \right)}{4\pi} \tag{11}$$

$$f_{Tp_p2} = \frac{\left(\frac{1}{r_s C_i} + \sqrt{\left(\frac{1}{r_s C_i} \right)^2 - \frac{4D^2}{LC_i}} \right)}{4\pi} \tag{12}$$

According to (10)–(12), the bode plot of the open loop transfer function can be drawn clearly, as shown in Figure 12. Obviously, there is a phase shift \Pr at the ripple current frequency r $ac\ f = 2\ f$. In order to reduce the phase shift to zero, the lead compensation circuit as shown in Figure 13 is used. In order to simplify the mathematical formulas and circuit diagrams, resistors and capacitors with the same resistance value or the same capacitance value are represented by the same component numbers. The transfer function of the lead compensation circuit can be defined as (13). In Figure 13, resistors R1, R2, R3, capacitor C1, and operational amplifier OPA1 create a zero frequency, as shown in Equation (14), and a pole frequency as shown in Equation (15), and its gain is shown in Equation (17). The resistor R4 and capacitor C2 and operational amplifiers OPA2 and OPA3 create a pole frequency as shown in Equation (16).

$$T_c(s) = \left(\frac{R_2}{R_1 + R_2} \right) \cdot \frac{1 + sR_1C_1}{\left(1 + s \frac{R_1R_2C_1}{R_1 + R_2} \right) \cdot (1 + sR_4C_2) \cdot (1 + sR_4C_2)}$$

The zeros, poles and gain of the lead compensation circuit can be expressed as

$$\text{Zero: } f_{Tc_z} = \frac{1}{2\pi C_1R_1}$$

$$\text{Pole } f_{Tc_p1} = \frac{1}{2\pi \frac{C_1R_1R_3}{R_3 + R_1}}$$

$$f_{Tc_p2} = \frac{1}{2\pi C_2R_4}$$

$$\text{Gain: } k_{Tc} = \frac{R_2}{R_1 + R_3}$$

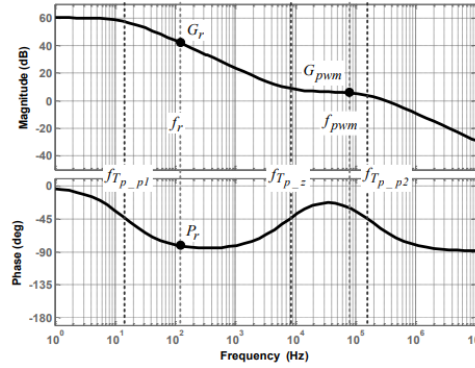


FIGURE 10. The bode plot of $T_p(s)$

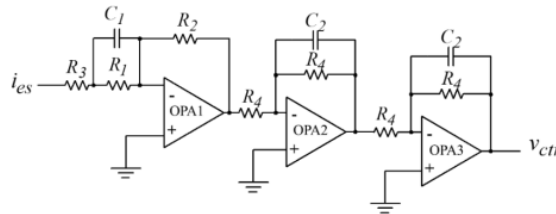


FIGURE 11. The lead compensation circuit

The compensation criteria are listen as following:

- 1.The gain margin and the phase margin should be large than 20dB and 45° to ensure the proposed system is stable.
- 2.The bandwidth should be larger than $r 10 f$ to ensure the proposed system can track the input current of the PV inverter.
- 3.The gain at switching frequency f_{pwm} should be smaller than -20dB to ensure the switching noise is small enough.
- 4.The phase shift $Prof$ the ripple current frequency should be close to zero to reduce the phase shift error at frequency rf .
- 5.To meet these compensation criteria, the frequencies of the zero and poles in the lead compensation circuit can be set as:

$$f_{Tc_z} = f_{Tp_p1},$$

$$f_{Tc_p1} = f_{Tp_z}, \text{ and}$$

$$f_{Tc_p2} = f_{Tp_p2}$$

In battery storage systems, there are many battery charging strategies which can be selected. In this design example, the general variable current charging strategy is used to minimize the control complexity.

IV. DESIGN EXAMPLE

In this section, the proposed BCSPD circuit prototype was developed to apply in a 1200 W PV system. Table 1 is the electrical specifications of the proposed system prototype. The circuit diagram of the BCSPD circuit prototype is shown in Figure 14. It was mainly constructed by a bidirectional DC/DC converter. The main components and parameters in the design example are listed in Table 2. A Microcontroller HT66F50 and operational am-plifier (OP Amp) TL084 are used as the control unit.

TABLE I ELECTRICAL SPECIFICATIONS OF THE PROPOSED SYSTEM

System Power P_o	1200 W
The MPP voltage of PV modules V_{PV}	150 V
The maximum regulation current $i_{cr}(t)$	± 8 A
Battery voltage V_b	48 V
Grid frequency f_{ac}	60 Hz
Ripple current frequency f_r	120 Hz

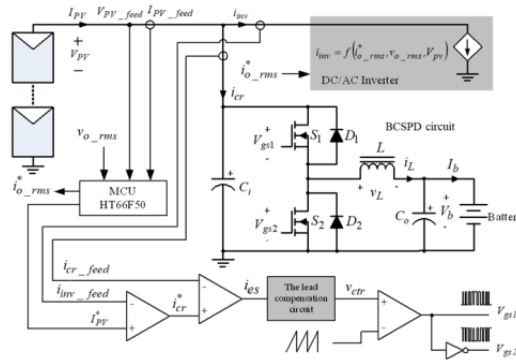


FIGURE 12. The configuration of the proposed BCSPD circuit

TABLE II MAIN COMPONENTS AND PARAMETERS

Power MOSFETs S_1 and S_2	IRF460
Microcontroller	HT66F50
OP Amp	TL084
Filter inductance L	100 μ H
Input capacitance C_i	10 μ F
Output capacitance C_o	100 μ F
Switch frequency f_{pwm}	80 kHz
Compensation resistance R_1	106 k Ω
Compensation resistance R_2	10.6 M Ω
Compensation resistance R_3	217 Ω
Compensation resistance R_4	1.3 k Ω
Compensation capacitance C_1	0.1 μ F
Compensation capacitance C_2	0.01 μ F

According to (14)–(17) and the component parameter in Table 2, frequencies of the zero and poles in the lead compensation circuit are

$$f_{Tc_z} = f_{Tp_p1} = 15 \text{ Hz,}$$

$$f_{Tc_p1} = f_{Tp_z} = 7.34 \text{ kHz}$$

$$f_{Tc_p2} = f_{Tp_p2} = 172.98 \text{ kHz.}$$

Thus, $R_1=106\text{k}\Omega$, $R_2=10.6\text{M}\Omega$, $R_3=217\Omega$, $R_4=1.3\text{k}\Omega$, $C_1=0.1\mu\text{F}$, $C_2=0.01\mu\text{F}$ are used in the compensation circuit. In order to reduce the PWM switching ripple current, (8) with ripple factor $r = 0.03$ is used. The input capacitor C_i can be obtained as $10\mu\text{F}$.

V. EXPERIMENTS

A 1200 W BCSPD circuit prototype was realized and shown as Figure 15 to assess system performance. Table 3 shows the used solar panel parameters. The experiment PV array was constructed by five solar panels connected in series.

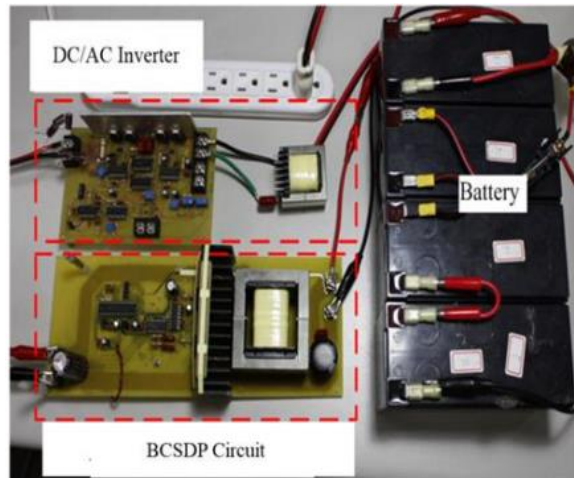


FIGURE 13. The realized 1200 W BCSPD circuit prototype

TABLE III THE SOLAR PANEL PARAMETERS

Maximum power	230 W
MPP voltage @1000 W/m ² , 25 °C	30 V
MPP current @1000 W/m ² , 25 °C	7 A
Module efficiency	13.4%
Solar cell efficiency	16.4%

Figure 16 is the bode plot of the close loop transfer function. From Figure 16, we can find that the gain margin, the phase margin and the bandwidth of the realized system are 23.6 dB, 81.4°, and 7.41 kHz. In addition, the gain and phase shift of the realized system at the ripple current frequency f_r are 6.72 dB and -1.33° , respectively. Figure 17 shows the regulation current control signal $*c_r i$ and the regulation current $c_r i$ with and without compensation. It is clear that the proposed BCSPD circuit can generate a completely complementary ripple current to reduce the PV modules current ripple as we wanted.

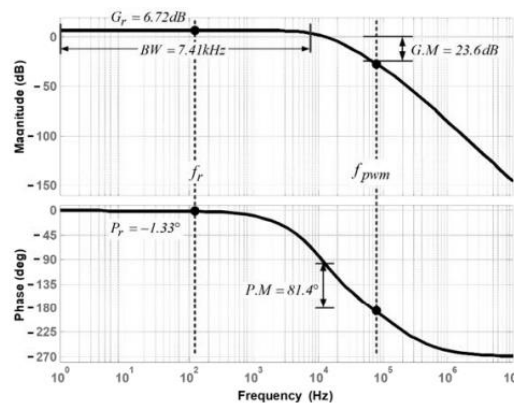


FIGURE 14. The close loop bode plot of the prototype

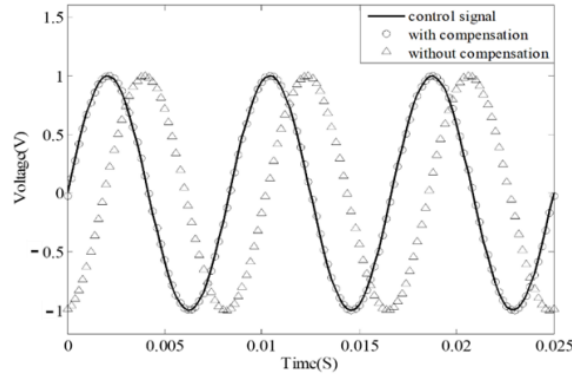


FIGURE 15. The regulation current control signal i^*_{cr} and the regulation current i_{cr} with and without compensation

In order to measure the voltage and current waveform, a digital 4-channel oscilloscope and three current probes are used. Figure 18 shows experiment waveforms of the PV power system without the current ripple reducing function. Clearly, the PV modules has a current ripple that is caused by the DC/AC inverter. The output ripple current of the PV modules ΔI_{PV} is 10A and the output ripple voltage of the PV modules ΔV_{PV} is 70 V. Therefore, the output power of PV modules is the time-variable value. The operation point of the PV modules does not operate at MPP. Figure 19 shows experiment waveforms of the proposed BCSPD circuit. We can see that the proposed BCSPD circuit can generate a completely complementary current ripple to reduce the PV modules current ripple from 10 A to 700 mA and the PV modules voltage ripple from 70 V to 5 V, obviously. The ripple current of the PV modules reduces to 3% and then the output power of the PV modules is increased.

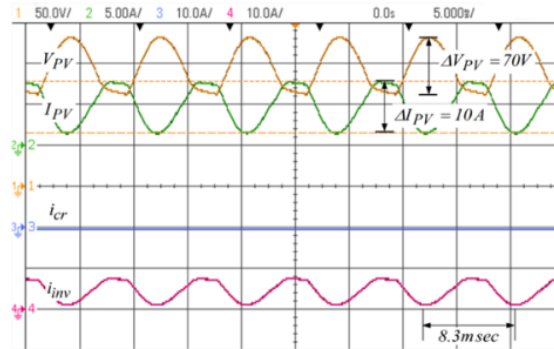


FIGURE 16. Experiment waveforms of the PV power system without the proposed BCSPD circuit

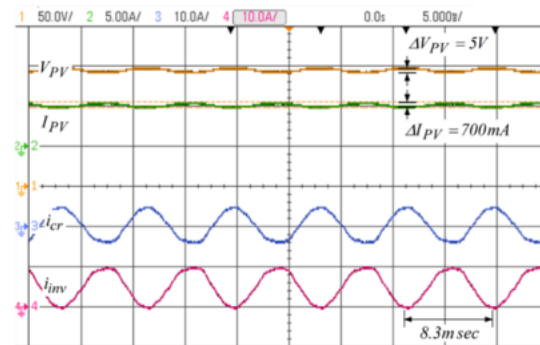


FIGURE 17. Experiment waveforms of the proposed BCSPD circuit

Figure 20 shows the measured waveforms when the prototype works in daytime. Clearly, the average current of the DC/AC inverter i_{inv} (i.e., 1 A) is smaller than the current of the MPP PV I (i.e., 5 A). We can see that the proposed

BCSPD circuit works as charger with 4 A. to make the PV modules work at MPP and the current ripple reducing is also maintained. Figure 21 shows the measured waveforms when the prototype work at night. The current of the MPP PV I is 0 A and the BCSPD circuit works as discharger with -3.5 A to make sure the utility power stability and the current ripple reducing is also maintained.

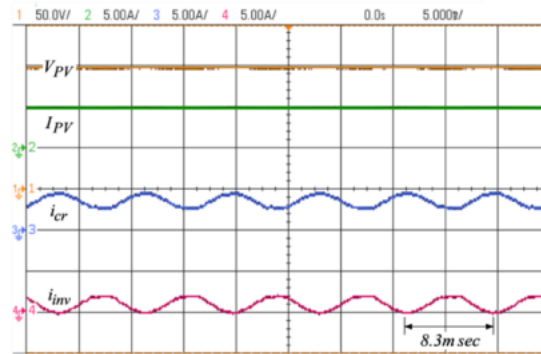


FIGURE 18. The measured waveforms when the proposed BCSPD circuit works in daytime

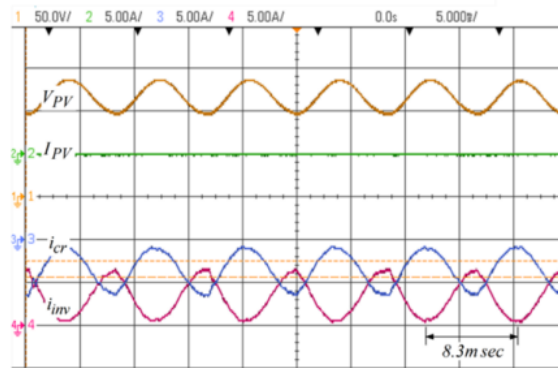


FIGURE 19. The measured waveforms when the proposed BCSPD circuit work at night

In order to measure the MPPT performance, a recorder is used to measure and recode the PV operating voltage and PV operating current. Figure 22 show the MPPT experiment results during the solar panel temperature is about 25 °C and the solar irradiance is varied in 700 W/m 2 – 800 W/m 2 range. The grey lines are the V-P curves of the used PV panel at solar irradiance = 700 W/m 2 and solar irradiance = 700 W/m 2 , respectively. The black spots are the measured operating points of PV. Note to that operating points of PV swings because of the solar irradiance is continuously varied. Clearly, the MPP is tracked from oscillating by the proposed system. This means that the double-line-frequency ripple current is eliminated, maximum output power of the PV system is obtained.

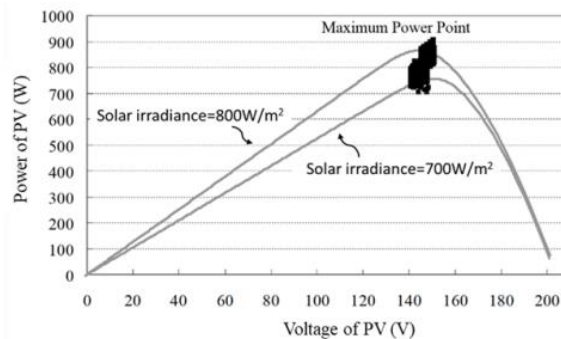


FIGURE 20. The 1200 W BCSPD circuit experiment result under solar irradiance is varied in 700 W/m 2 – 800 W/m 2 range

VI. CONCLUSIONS

A traditional PV inverter is divided into single-stage and two-stage. Although the single-stage PV inverter has high power conversion efficiency, it has the problem of low-frequency ripple in PV. This causes a decrease in the efficiency of PV power generation. The two-stage PV inverter can be buffered by a DC bus without the problem of low-frequency ripple. Therefore, the efficiency of PV power generation is high. However, the two-stage PV inverter has one more series-connected DC/DC converter than the single-stage PV inverter, so the power conversion efficiency is low. In order to overcome the above problem, a novel CS-MPPT with ripple-reducing technology for PV power applications was successfully proposed in this paper. The proposed system is a parallel-connected structure, so its power conversion efficiency is as high as that of a single-stage PV inverter. In addition, the proposed CS-MPPT can track the MPP, regulate the load power condition and reduce current ripple at the same time. Therefore, a high efficiency of PV power generation is also obtained. In order to assess the proposed system performance, a 1200 W prototype was designed and implemented. Experiment results show that the proposed CSMPPT with ripple reducing system can generate a completely complementary current ripple to reduce the PV modules current ripple from 10 A to 700 mA and the PV modules voltage ripple from 70 V to 5 V, obviously. Thus, the power efficiency of the PV modules is increased as theoretical prediction. The feasibility and excellent performance of the proposed CS-MPPT with ripple reducing system are verified by experiment results.

A novel BCSPD technology for PV power applications was successfully proposed in this paper. The proposed system is a parallel-connected structure, so its power conversion efficiency is as high as that of a single-stage PV inverter. In addition, the proposed CS-MPPT can track the MPP, regulate the load power condition and reduce current ripple at the same time. Therefore, a high output power of PV power generation is also obtained. In order to assess the proposed system performance, a 1200 W prototype was designed and implemented. Experiment results show that the proposed BCSPD circuit can generate a completely complementary current ripple to reduce the PV modules current ripple from 10 A to 700 mA and the PV modules voltage ripple from 70 V to 5 V, obviously. Thus, the output power of the PV modules is increased as theoretical prediction. The feasibility and excellent performance of the proposed BCSPD circuit are verified by experiment results.

REFERENCES

1. I. Vairavasundaram, V. Varadarajan, P. J. Pavankumar, R. K. Kanagavel, L. Ravi and S. Vairavasundaram, "A review on small power rating PV inverter topologies and smart PV inverters", in *Electronics*, vol. 10, 2021.
2. M. N. H. Khan, M. Forouzesh, Y. P. Siwakoti, L. Li, T. Kerekes and F. Blaabjerg, "Transformerless Inverter Topologies for Single-Phase Photovoltaic Systems: A Comparative Review", in *IEEE Journal of Emerging and Selected Topics in Power Electronics*, vol. 8, no. 1, pp. 805-835, March 2020, doi: 10.1109/JESTPE.2019.2908672.
3. B. K. Santhoshi, K. M. Sundaram, S. Padmanaban, J. B. Holm-Nielsen and K.K. Prabhakaran, "Critical review of PV grid-tied inverters", *Energies*, vol. 12, no. 10, pp. 1-26, 2019.
4. M. Y. Ali Khan, H. Liu, Z. Yang and X. Yuan, "A comprehensive review on grid connected photovoltaic inverters their modulation techniques and control strategies", *Energies*, vol. 13, no. 16, pp. 4185, Aug. 2020.
5. K. Zeb, W. Uddin, Muhammad A. Khan, Z. Ali, M. U. Ali, N. Christofides et al., "A comprehensive review on inverter topologies and control strategies for grid connected photovoltaic system", *Renewable and Sustainable Energy Reviews*, vol. 94, pp. 1120-1141, 2018.
6. H. Hu, S. Harb, N. Kutkut, I. Batarseh and Z. J. Shen, "A Review of Power Decoupling Techniques for Microinverters With Three Different Decoupling Capacitor Locations in PV Systems", *IEEE Transactions on Power Electronics*, vol. 28, no. 6, pp. 2711-2726, June 2013, doi: 10.1109/TPEL.2012.2221482.
7. P. T. Krein, R. S. Balog and M. Mirjafari, "Minimum Energy and Capacitance Requirements for Single-Phase Inverters and Rectifiers Using a Ripple Port", in *IEEE Transactions on Power Electronics*, vol. 27, no. 11, pp. 4690-4698, Nov. 2012, doi: 10.1109/TPEL.2012.2186640.
8. A. R. Gautam, D. M. Fulwani, R. R. Makineni, A. K. Rathore and D. Singh, "Control Strategies and Power Decoupling Topologies to Mitigate 2ω -Ripple in Single-Phase Inverters: A Review and Open Challenges," *IEEE Access*, vol. 8, pp. 147533-147559, 2020, doi: 10.1109/ACCESS.2020.3015315.
9. L. Zhang, X. Ruan and X. Ren, "Second-Harmonic Current Reduction and Dynamic Performance Improvement in the Two-Stage Inverters: An Output Impedance Perspective", in *IEEE Transactions on Industrial Electronics*, vol. 62, no. 1, pp. 394-404, Jan. 2015, doi: 10.1109/TIE.2014.2331015.

10. M. Y. A. Khan, H. Liu, S. Habib, D. Khan, X. Yuan. " Design and performance evaluation of a step-up DC–DC converter with dual loop controllers for two stages grid connected PV inverter. Sustainability", in Sustainability, vol. 14, Iss. 2, 2022, doi: 10.3390/su14020811.
11. G. C. Christidis, A. C. Kyritsis, N. P. Papanikolaou and E. C. Tatakis, "Investigation of Parallel Active Filters' Limitations for Power Decoupling on Single-Stage/Single-Phase Microinverters", in IEEE Journal of Emerging and Selected Topics in Power Electronics, vol. 4, no. 3, pp. 1096-1106, Sept. 2016, doi: 10.1109/JESTPE.2016.2552980.
12. H. Watanabe, T. Sakuraba, K. Furukawa, K. Kusaka and J. Itoh, "Development of DC to Single-Phase AC Voltage Source Inverter With Active Power Decoupling Based on Flying Capacitor DC/DC Converter", in IEEE Transactions on Power Electronics, vol. 33, no. 6, pp. 4992-5004, June 2018, doi: 10.1109/TPEL.2017.2727063.
13. S. Bhowmick and L. Umanand, "Design and Analysis of the Low Device Stress Active Power Decoupling for Single-Phase Grid Connection for a Wide Range of Power Factor", in IEEE Journal of Emerging and Selected Topics in Power Electronics, vol. 6, no. 4, pp. 1921-1931, Dec. 2018, doi: 10.1109/JESTPE.2018.2794784.
14. Y. C. Chen, L. R. Chen, C. M. Lai, Y. C. Lin, T. J. Kuo. " Development of a DC-Side Direct Current Controlled Active Ripple Filter for Eliminating the Double-Line-Frequency Current Ripple in a SinglePhase DC/AC Conversion System", in Energies, vol. 13, no. 18, 2020, doi: 10.3390/en13184772.
15. Z. Yang, J. Zeng, Q. Zhang, Z. Zhang, V. Winstead and D. Yu, "A Composite Power Decoupling Method for a PV Inverter With Optimized Energy Buffer", in IEEE Transactions on Industry Applications, vol. 57, no. 4, pp. 3877-3887, July-Aug. 2021, doi: 10.1109/TIA.2021.3079162.